BIOCHEMISTRY
including biophysical chemistry & molecular biology
Article

*Biochemistry* **2010,** *49,* 7151–7163 7151
DOI: 10.1021/bi100824v

# Kinetic Mechanism and Rate-Limiting Steps of Focal Adhesion Kinase-1

Jessica L. Schneck,[‡] Jacques Briand,[§] Stephanie Chen,[‡] Ruth Lehr,[‡] Patrick McDevitt,[‡] Baoguang Zhao,[∥] Angela Smallwood,[∥] Nestor Concha,[∥] Khyati Oza,[‡] Robert Kirkpatrick,[‡] Kang Yan,[⊥] James P. Villa,[‡] Thomas D. Meek,*[,‡] and Sara H. Thrall[‡]

[‡]*Departments of Biological Reagents and Assay Development,* [§]*Analytical Chemistry, and* [∥]*Computational and Structural Chemistry, GlaxoSmithKline Pharmaceuticals, 1250 South Collegeville Road, Collegeville, Pennsylvania 19426-0989, and* [⊥]*Chemizon, Inc., Minzhuang Road 3, Haidian District, Beijing, 100195 China*

*Received May 24, 2010; Revised Manuscript Received June 24, 2010*

ABSTRACT: Steady-state kinetic analysis of focal adhesion kinase-1 (FAK1) was performed using radiometric measurement of phosphorylation of a synthetic peptide substrate (Ac-RRRRRRSETDD**Y**AEIID-$NH_2$, FAK-tide) which corresponds to the sequence of an autophosphorylation site in FAK1. Initial velocity studies were consistent with a sequential kinetic mechanism, for which apparent kinetic values $k_{cat}$ ($0.052 \pm 0.001\ s^{-1}$), $K_{MgATP}$ ($1.2 \pm 0.1\ \mu M$), $K_{iMgATP}$ ($1.3 \pm 0.2\ \mu M$), $K_{FAK\text{-}tide}$ ($5.6 \pm 0.4\ \mu M$), and $K_{iFAK\text{-}tide}$ ($6.1 \pm 1.1\ \mu M$) were obtained. Product and dead-end inhibition data indicated that enzymatic phosphorylation of FAK-tide by FAK1 was best described by a random bi bi kinetic mechanism, for which both E-MgADP-FAK-tide and E-MgATP-P-FAK-tide dead-end complexes form. FAK1 catalyzed the $\beta\gamma$-bridge:$\beta$-non-bridge positional oxygen exchange of [$\gamma$-$^{18}O_4$]ATP in the presence of 1 mM [$\gamma$-$^{18}O_4$]ATP and 1.5 mM FAK-tide with a progressive time course which was commensurate with catalysis, resulting in a rate of exchange to catalysis of $k_x/k_{cat} = 0.14 \pm 0.01$. These results indicate that phosphoryl transfer is reversible and that a slow kinetic step follows formation of the E-MgADP-P-FAK-tide complex. Further kinetic studies performed in the presence of the microscopic viscosogen sucrose revealed that solvent viscosity had no effect on $k_{cat}/K_{FAK\text{-}tide}$, while $k_{cat}$ and $k_{cat}/K_{MgATP}$ were both decreased linearly at increasing solvent viscosity. Crystallographic characterization of inactive versus AMP-PNP-liganded structures of FAK1 showed that a large conformational motion of the activation loop upon ATP binding may be an essential step during catalysis and would explain the viscosity effect observed on $k_{cat}/K_m$ for MgATP but not on $k_{cat}/K_m$ for FAK-tide. From the positional isotope exchange, viscosity, and structural data it may be concluded that enzyme turnover ($k_{cat}$) is rate-limited by both reversible phosphoryl group transfer ($k_{forward} \approx 0.2\ s^{-1}$ and $k_{reverse} \approx 0.04\ s^{-1}$) and a slow step ($k_{conf} \approx 0.1\ s^{-1}$) which is probably the opening of the activation loop after phosphoryl group transfer but preceding product release.

Focal adhesion kinase-1 (FAK1)[1] is a nonreceptor tyrosine kinase which is virtually ubiquitous in cells (*1*). The primary role of FAK1 is the conductance of signals from activated integrin receptors to intracellular protein kinase cascades by either phosphorylation or localization of its downstream effectors, which ultimately leads to activation of the ERK and JNK/MAPK pathways (*2*). Association of FAK1 and several signaling proteins, such as Src-family tyrosine kinases, $p130^{Cas}$, Shc, Grb2, PI3-kinase, paxillin, and tallin, has been demonstrated (*2*). Signal transduction through FAK1 indirectly plays a critical role in many cellular processes, such as cell cycle regulation, cadherin-dependent cell adhesion, migration, invasion, and metastasis, and apoptosis (*3*). Specifically, FAK1 is involved in the assembly/disassembly of cellular adhesion sites, which are vital in the control of cell migration. Increased expression of FAK1 has been observed in a variety of human cancers, including thyroid, prostate, cervical, colon, rectal, oral epithelial, melanoma, and ovarian cancers (*1*, *3*). Amplified FAK1 expression and activity are correlated with malignant or metastatic disease and at stages of the diseases which comprise poor prognosis (*3*, *4*).

FAK1 is a homodimeric protein consisting of 119-kDa subunits (*2*). The catalytic domain of FAK1 contains a SH2 (Src homology 2) motif and is flanked by a large N-terminal FERM (band *f*our-point-one, *e*rzin, *r*adixin, *m*oesin homology) domain and a C-terminal domain containing the focal adhesion targeting (FAT) sequence (*5*). When FAK1 is in its inactive form, the FERM domain bridges the N- and C-lobes of the kinase domain and extends across the active site cleft, blocking access to substrate and thereby ultimately hindering catalysis (*5*). The FAT domain consists of a four-helix bundle (*6*, *7*), and this domain is critical for targeting to focal adhesions via association with paxillin (*5*).

Src kinase activates FAK1 by phosphorylating Tyr576 and Tyr577 residues in the activation loop of the enzyme (amino acids 564−584), which triggers autophosphorylation of the FAK1 protein at Tyr397 (*8*). This autophosphorylation, which can be

*To whom correspondence should be addressed. Phone: (610) 917-6786. Fax: (610) 917-7385. E-mail: Thomas.D.Meek@gsk.com.

[1]Abbreviations: AMP-PNP, adenosine 5′-($\beta$,$\gamma$-imido)triphosphate; DTT, dithiothreitol; EDTA, ethylenediaminetetraacetic acid; FAK1, focal adhesion kinase-1; FAK-tide, Ac-RRRRRRSETDD**Y**AEIID-$NH_2$; G6PDH, glucose-6-phosphate dehydrogenase; GST-Src, glutathione transferase N-terminally tagged Src kinase; HEPES, 4-(2-hydroxyethyl)-1-piperazineethanesulfonic acid; HK, yeast hexokinase; LC/MS/MS, liquid chromatography, tandem mass spectrometry; LDH, porcine heart lactate dehydrogenase; P-FAK-tide, H-SETDD(**phosphoY**)AEIID-OH; PBS, phosphate-buffered saline; PEP, phosphoenolpyruvate; PIX, positional isotope exchange; PK, rabbit muscle pyruvate kinase; TCEP, tris(2-carboxyethyl)phosphine.


Published on Web 07/02/2010

cis or trans phosphorylation, is required for full activation of the kinase domain (*9*). FAK1 is unique among kinases in that Tyr397 is not located in the activation loop but rather in a linker region between the N-terminal FERM domain and the catalytic domain (*9*). Natural substrates for FAK1 include paxillin and $p130^{Cas}$ (*2*).

The detailed kinetic mechanisms of several protein kinases involved in signal transduction have been elucidated. Two examples include Csk (*10*) and ERK2 (*11*, *12*). Csk and ERK2 both employ a random bi bi reaction mechanism for which release of the MgADP product is mostly rate-determining. A thorough understanding of the kinetic mechanism of FAK could greatly augment the proper design and execution of high-throughput screening assays intended to find mechanistically novel inhibitors which target the rate-limiting step(s) of catalysis. In this study initial velocity, dead-end and product inhibition, positional isotope exchange of MgATP, solvent viscometric, and structural studies were undertaken to characterize the catalytic mechanism of FAK1 using FAK-tide, a septidecapeptide of the sequence Ac-RRRRRRSETDD**Y**AEIID-$NH_2$, which is a mimic of the autophosphorylation site of FAK1 containing Tyr397.

## MATERIALS AND METHODS

*Materials*. HEPES, DTT, ATP, and ADP were purchased from Invitrogen. Magnesium chloride, manganese chloride, Tween-20, KCl, NADH, PK, PEP, glucose, and sucrose were purchased from Sigma-Aldrich. AMP-PNP was purchased from Roche. $NAD^+$, HK, and G6PDH were purchased from Calbiochem. LDH was purchased from USB Corp. Ficoll 400 was purchased from Alfa Aesar. FAK-tide (Ac-RRRRRRSETDDYAEIID-$NH_2$) was purchased from 21st Century Biochemicals, Inc. (purity ≥95%). Phospho-FAK-tide (H-SETDD-(**phosphoY**)AEIID-OH) and Phe/Tyr-FAK-tide (H-SETDD-**F**AEIID-OH) were purchased from California Peptide at >99% purity. Phosphocellulose filter paper plates (96-well) were purchased from Millipore. [$\gamma$-$^{33}$P]ATP (10 $\mu$Ci/$\mu$L specific activity, diluted to 2−120 nCi/$\mu$L for assays) and Microscint-20 were obtained from Perkin-Elmer. Reactions were conducted in 96-well half-area, nonbinding surface plates purchased from Corning, Inc.

*Preparation of* [$\gamma$-$^{18}$*O*]*ATP*. [$\gamma$-$^{18}$O]ATP was provided by WuXi (Shanghai, China) by coupling of the mono(tri-*n*-butylammonium) salt (*13*) of [$^{18}O_4$]phosphate, prepared from $PCl_5$ and [$^{18}$O]$H_2O$ (*14*), with ADP-morpholidate (*15*). The resulting tris(triethylammonium salt) of [$\gamma$-$^{18}O_4$]ATP was found to be >96% pure by high-performance liquid chromatography and with a molecular mass of 818.75 amu as determined by mass spectrometry. Further quantification of the product [$\gamma$-$^{18}$O]ATP was ascertained from measurement of a sample by its absorbance at 259 nm for total adenine content and also by enzymatic conversion of ATP to ADP by use of the hexokinase/glucose-6-phosphate dehydrogenase coupling enzyme system as described (*17*). Samples were found to consist of ≥93% ATP. Analysis of the integrals of $\gamma$-phosphate resonance of the [$\gamma$-$^{18}O_4$]ATP by $^{31}$P NMR indicated that the substitution pattern of $^{18}$O atoms in the $\gamma$-phosphate group was as follows: [$\gamma$-$^{18}O_4$], 74.4%; [$\gamma$-$^{18}O_3{}^{16}$O], 25.6% (*16*).

*Enzyme Preparation*. Full-length human FAK1 (NM_153831) was cloned into a baculovirus expression vector derived from pDest8 (Invitrogen) containing an N-terminal FLAG epitope tag followed by a hexahistidine tag and a TEV protease cleavage site. FLAG-6×His-TEV-FAK1 was generated using the Bac-to-Bac (Invitrogen), and the protein was expressed in a proprietary Sf9 insect cell line. Cells were grown to a density of $4 \times 10^6$ cells/mL in 10 L and infected with Flag-6×His-TEV-FAK1 virus at a multiplicity of infection factor of 2.8. At 48 h postinfection, cells were harvested by centrifugation at 1200 rpm for 20 min. The baculovirus-expressed protein was solubilized from 60 g of cells by sonication in 50 mM Tris buffer (pH 7.5) containing 300 mM NaCl, 0.1 mM TCEP, and 1% Triton (v/v) (lysis buffer) and purified by batch binding to 7.5 mL of NiNTA agarose resin (Qiagen) equilibrated in lysis buffer. The resin was washed with 10 mM imidazole in lysis buffer with 0.1% Triton, and the FAK1 protein was eluted with 10 column volumes of a linear gradient from 10 to 300 mM imidazole in wash buffer. The eluted protein was concentrated and subjected to size-exclusion chromatography on a 300 mL SDX200 column (2.6 × 60 cm) (GE Healthcare) equilibrated with 50 mM Tris (pH 7.5), 200 mM NaCl, and 0.1% Triton, to remove aggregated protein. All steps were performed at 4 °C.

The collected fractions corresponding to FAK1 were activated with recombinant HisSBP-Src (SBP is streptavidin binding protein) at a 1:20 (w/w) ratio of Src to FAK1 in the presence of 20 mM $MgCl_2$, 2 mM ATP, and 2 mM DTT. The reaction was incubated at room temperature for 3 h and then overnight at 4 °C, after which Src protein was removed from the reaction by binding of its SBP tag to streptavidin resin. The activated FAK protein was chromatographed on a SDX200 column as above to remove any aggregated protein resulting from the activation. This procedure resulted in almost complete phosphorylation of Tyr-576 and Tyr-577 as determined by LC/MS/MS analysis. Phosphorylation of these two residues is required for fully active FAK1.

The gene that was synthesized for the coding sequence of the FAK1 kinase domain (411−686) was optimized in terms of codon usage and also contains a 5′ fused sequence encoding an N-terminal Tev cleavage site (Supporting Information Figure 1S) and was transferred by Gateway BP recombination into pDONR221 (Invitrogen). The Tev-FAK1(411−686) coding sequence was subsequently transferred by Gateway LR recombination into pDEST8$His_6$, a modified version of the Invitrogen pDEST8 baculovirus destination vector containing an N-terminal $His_6$ tag module in frame with the Gateway cassette. The resultant construct encodes $His_6$TevFAK1(411−686) with the following N-terminal His6tev linker preceding serine-411 of FAK1 (MGHHHHHHTSTSLYKKAGFENLYFQG). This destination plasmid was used to generate recombinant baculovirus expressing $His_6$TevFAK1(411−686) using the Bac-to-Bac baculovirus expression system (Invitrogen). The protein was expressed in a high cell density optimized Sf9 insect cell line (S9). Cells were infected at $1 \times 10^6$ cells/mL viable cell concentration with frozen baculovirus infected insect cells (BIIC) and harvested at 65 h postinfection.

Frozen baculovirus-infected S9 cells expressing $His_6$Tev-FAK1(411−686) were dispersed (1 g of cells/10 mL of buffer) in buffer A (50 mM Tris-HCl, 0.5 M NaCl, 10 mM imidazole, 5 mM 2-mercaptoethanol, 5% glycerol, pH 7.6) containing protease inhibitors (Roche complete, no EDTA) and 1 mM PMSF. Cells were lysed by two passes at 10000 psi through a M110Y fluidizer (Microfluidics Inc., Newton, MA) and clarified by centrifugation for 1 h at 35000*g*. The supernatant was applied to a NiNTA column (Qiagen Inc.) equilibrated in buffer A, washed with 10 column volumes of buffer A, and eluted with

0.25 M imidazole in buffer A. Fractions containing FAK1 kinase domain were pooled and treated with Tev protease (1:10 ratio) to remove hexaHis tag. The reaction mixture was fractionated on a Superdex 200 column in buffer B (40 mM Tris-HCl, 0.15 M NaCl, 5% glycerol, 1 mM DTT, pH 7.6). FAK1 kinase domain was eluted as a monomer from a Superdex 200 column. LC/MS mass determination indicated unphosphorylated FAK1. FAK1 kinase domain was activated with His-GST-cSrc (constitutively active cSrc, 86−537, Y530F) in buffer B containing 10 mM ATP, 20 mM $MgCl_2$, 10 mM DTT, and 10 mM $\beta$-glycerophosphate (1:30 ratio) at 30 °C, monitoring phosphorylation by LC/MS. His-GST-cSrc was removed by passage through a NiNTA column. FAK1 solution was further fractionated on Source 15S in buffer C (50 mM sodium acetate, 1 mM TCEP, 1 mM glycerophosphate, 1 mM EDTA, 5% glycerol, pH 5.5) with a 20 mM to 0.5 M NaCl gradient. The major peak containing a diphosphorylated form of FAK1 (observed mass of 31982 Da against calculated mass of 31815 Da) was pooled, dialyzed against the final storage buffer (50 mM Tris-HCl, 0.25 M NaCl, 2 mM TCEP, 1 mM EDTA, 5% glycerol, pH 7.5), and snap-frozen in liquid $N_2$ for storage at −80 °C.

*Steady-State Kinetic Assays*. Steady-state kinetic parameters were obtained using a filter-binding assay which measured phosphorylation of the tyrosyl residue of FAK-tide peptide from [$\gamma$-$^{33}$P]ATP. Initial rate studies of full-length FAK1 were performed in 40 $\mu$L solutions containing 40 mM HEPES (pH 7.2), 10 mM $MgCl_2$, 2 mM $MnCl_2$, 1 mM DTT, 0.01% (v/v) Tween-20 buffer, 800 pM FAK1, FAK-tide (0.5−250 $\mu$M), and [$\gamma$-$^{33}$P]ATP (2−120 nCi/$\mu$L, 0.1−10 $\mu$M ATP) in half-area, 96-well plates (21 ± 1 °C). Reactions were quenched at 0−60 min with 40 $\mu$L of 1% (v/v) $H_3PO_4$, and reaction mixtures were transferred to 96-well plates containing phosphocellulose filter papers. After 20 min incubation, filter wells were washed three times with 0.5% (v/v) $H_3PO_4$ and then incubated at 50 °C for 30 min. MicroScint-20 (50 $\mu$L) was added to each dried well, and the amount of [$\gamma$-$^{33}$P]-labeled peptide was quantified by scintillation counting on a TopCount instrument (Perkin-Elmer). Total input picomoles of [$\gamma$-$^{33}$P]ATP, assuming quantitative capture of radioactivity, was determined for each filter plate by generation of a calibration curve comprised of enzyme-free reaction mixtures. For all data at all combinations of substrate concentrations tested, the linearity of the reaction time course was determined via individual time points taken at 10 min intervals at 0−80 min. All combinations of substrate concentrations tested appeared linear for at least 60 min, and initial rates were obtained from analysis of the initial linear phases.

Initial rates were also assessed by use of the PK-LDH coupled-enzyme system to measure amounts of MgADP formed from FAK-tide and MgATP as catalyzed by FAK1. Briefly, 2−25 $\mu$L aliquots were withdrawn at intervals of 0−80 min from 1.0 mL reaction mixtures (21 ± 1 °C) containing 40 mM HEPES (pH 7.2), 10 mM $MgCl_2$, 3 mM DTT, 0−1 mM MgATP, 0−1.5 mM FAK-tide, and 0.1 $\mu$M FAK1. The concentrations of MgADP were quantified by measurement of the decrease in NADH absorbance (340 nm) on a Spectramax spectrophotometer in a 48 $\mu$L reaction mixture (384-well clear-bottom Greiner plate) containing 100 mM HEPES (pH 7.2), 100 mM KCl, 20 mM $MgCl_2$, 2 mM PEP, 200 $\mu$M NADH, 25 units/mL LDH, and 25 units/mL PK, and resulting MgADP concentrations were determined from a calibration curve. This coupled-enzyme assay was also used to quantify the MgADP produced in the samples for PIX.

Likewise, initial rates for the reverse reaction, or for quantification of MgATP concentrations within reaction mixtures for PIX, were determined using the HK-G6PDH enzyme-coupling system. In a 384-well clear bottom Greiner plate, 48 $\mu$L reaction mixtures comprised of 100 mM HEPES (pH 7.2), 100 mM KCl, 20 mM $MgCl_2$, 2 mM $NAD^+$, 10 units/mL G6PDH, and 25 units/mL HK were used to detect the remaining concentrations of [$\gamma$-$^{18}$O]MgATP with 2 or 25 $\mu$L aliquots taken from reaction mixtures (21 ± 1 °C). Reactions were initiated by addition of 1 $\mu$L of 50 mM glucose, and as above, [MgATP] was determined from a calibration curve.

For viscosity studies, solutions of 0−40% (w/v) sucrose or 0−10% (w/v) Ficoll 400 in 40 mM HEPES (pH 7.2), 10 mM $MgCl_2$, 2 mM $MnCl_2$, 1 mM DTT, and 0.01% (v/v) Tween-20 buffer were prepared, and the resulting viscosity was measured by an Oswalt viscometer. Initial velocity data were then determined to obtain kinetic parameters for the two substrates in the presence of 0−40% ($\eta_{rel}$ = 1−3.8) sucrose or 0−10% ($\eta_{rel}$ = 1−4.5) Ficoll 400 using the filtration binding assay at saturating fixed substrate concentrations (12 $\mu$M MgATP or 25 $\mu$M FAK-tide).

*Positional Isotope Exchange in [$\gamma$-$^{18}$O]ATP*. In a 1.0 mL reaction mixture, 100 nM full-length FAK was incubated with 40 mM HEPES (pH 7.2), 10 mM $MgCl_2$, 1 mM DTT, 1 mM [$\gamma$-$^{18}$O]ATP, and 1.5 mM FAK-tide at 21 ± 1 °C for 70−250 min. The reaction mixtures were quenched by adding 0.25 mL of 0.5 M EDTA (pH 8.0), followed by vigorous mixing. The extent of $\beta\gamma$-bridge:$\beta$-nonbridge positional oxygen exchange in [$\gamma$-$^{18}$O]ATP was determined from the peak intensities of $^{31}$P NMR signals of the [$\gamma$-$^{18}O_4$]-P and [$\gamma$-$^{18}O_3{}^{16}$O]-P and [$\beta$-$^{18}$O$^{16}O_3$]-P and [$\beta$-$^{16}O_4$]-P species, owing to the ≈0.02 ppm change in chemical shift of the $^{31}$P species resulting from substitution of an $^{16}$O ligand by $^{18}$O (*16*). NMR samples were prepared by mixing together 450 $\mu$L of the quenched reaction mixtures, 60 $\mu$L of $D_2O$, and 90 $\mu$L of 0.5 M EDTA yielding the final sample conditions: 0.6 mM combined [$\gamma$-$^{18}$O]ATP + [$\beta$-$^{18}$O]ADP, 24 mM HEPES (pH 7.2), 6 mM $MgCl_2$, 60 nM FAK1, 0.9 mM FAK-tide, 10% (v/v) $D_2O$, and 150 mM EDTA in a volume of 600 $\mu$L. The $^{31}$P NMR spectra were measured by using a Varian Unity INOVA 600 operating at 242.76 MHz. All of the spectra were recorded using a 5 mm probe regulated at 25 °C, 32K data points, a sweep width of 20000 Hz, an acquisition time of 1.6384 s, 16384 scans, and a relaxation delay of 0.1 s. Prior to Fourier transformation, the resolution was enhanced by applying a shifted sine bell (36°) over the first 32K data. In addition to the spectral quantification, ADP formation and residual ATP in each of the quenched samples were also quantified enzymatically to assess the extent of the FAK reaction using respectively the PK-LDH and HK-G6PDH coupling systems as described above and in Meek et al. (*17*).

*Crystallization and Structural Characterization of AMP-PNP-Bound FAK1*. Crystals of the catalytic domain of human FAK1 (residues 411−686) in complex with the nonhydrolyzable ATP analogue, AMP-PNP (adenosine 5′-($\beta$,$\gamma$-imido)triphosphate), and $Mg^{2+}$ were grown by sitting-drop vapor diffusion at 20 °C from a solution of 18−21% polyethylene glycol 3350 and 0.2 M lithium sulfate buffered with 0.1 M Tris-HCl (pH 8.5). $MgCl_2$ and AMP-PNP were added to the FAK1 enzyme solution immediately before crystallization to give a final concentration of 3 mM. Crystals started to appear after 2 weeks and attained full size after 6 weeks, by which time they were harvested, allowed to equilibrate in a similar crystallization solution, now containing 18% ethylene glycol, and quick

frozen in liquid nitrogen. X-ray diffraction data to 1.45 Å resolution were collected using the MAR-USA CCD165 detector at the Industrial Macromolecular Crystallography Association beamline 17-ID in the Advanced Photon Source at Argonne National Laboratory (Chicago, IL). Diffraction data were indexed and scaled using the HKL2000 software (*18*) (see Table 4). The crystals belong to the monoclinic space group $P2_1$, with two molecules of the binary complex FAK/AMP-PNP in the asymmetric unit. The structure of the complex was determined by the molecular replacement method using the published coordinates of FAK with ADP (PDB: 1MP8) (*19*) using the program Phaser (*20*). The graphic program Coot (*21*) was used to make manual adjustments to the model. The structure has been refined to 1.45 Å resolution using REFMAC5 (*22*) to a final crystallographic *R*-value of 0.23 and a free *R*-value of 0.24. The final structure includes two FAK1 molecules (chain A residues from 414 to 686 and chain B residues from 415 to 686) each bound with one AMP-PNP molecule, one sulfate ion, and 201 water molecules (Table 4).

*Data Analysis*. Initial velocity data for FAK1 were fitted to eq 1 or 2, for single substrate and bisubstrate kinetics, respectively, using Grafit 5.0.8 (Erithacus Software Ltd.)

$$v = VA/(K_a + A) \quad (1)$$

$$v = VAB/(K_{ia}K_b + K_bA + K_aB + AB) \quad (2)$$

for which V is the maximal velocity, A is the concentration of MgATP, B is concentration of FAK-tide, $K_a$ and $K_b$ are apparent Michaelis constants, and $K_{ia}$ is the apparent dissociation constant for MgATP.

Product and dead-end inhibition studies apparently conforming to competitive and noncompetitive inhibition were fitted to eqs 3 and 4, respectively

$$v = VA/[K_a(1 + I/K_{is}) + A] \quad (3)$$

$$v = VA/[K_a(1 + I/K_{is}) + A(1 + I/K_{ii})] \quad (4)$$

where $K_{is}$ and $K_{ii}$ are respectively the apparent slope and intercept inhibition constants.

The effect of viscosogens on the initial velocity data of FAK1 in double-reciprocal form was fitted to either eq 5 or 6

$$1/v = (1/k_a)(1/A)\eta_{rel} + 1/k_c + \eta_{rel}/k_d \quad (5)$$

$$1/v = (1/k_a + \eta_{rel}/k_b)(1/A) + 1/k_c + \eta_{rel}/k_d \quad (6)$$

for which A is either of the substrates, $\eta_{rel}$ is the relative viscosity, V is the maximal velocity, and $k_a$, $k_b$, $k_c$, and $k_d$ are respectively collections of individual rate constants found in the expressions for $K_a/V$ and $1/V$, which are dependent upon the mechanism and substrate.

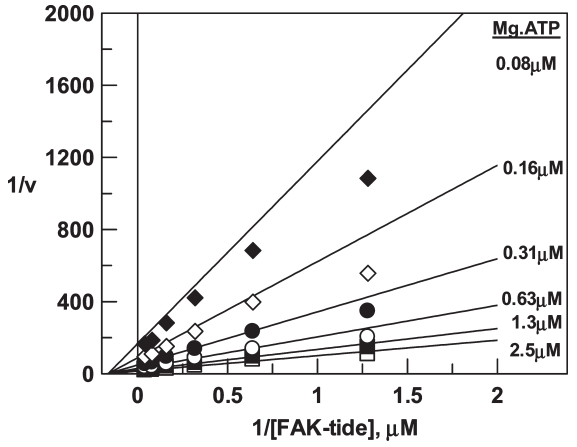


FIGURE 1: Initial velocity of the FAK1-catalyzed reaction. Experimental initial rates were fitted to eq 2 as described in Materials and Methods, and shown in double-reciprocal format, where v represents picomoles of product per minute, and with variable concentrations of FAK-tide at changing fixed concentrations of MgATP.

## RESULTS AND DISCUSSION

*Initial Velocity Studies*. Initial rate data for the FAK1-catalyzed reaction conformed to standard Michaelis−Menten kinetics with either MgATP or FAK-tide as the variable substrate, which were evaluated by fitting of data to eq 1 over a wide range of concentrations ($0.2-5K_m$) (data not shown). An initial velocity study was then performed, for which the double-reciprocal plot is shown (Figure 1). The resulting intersecting initial velocity pattern of FAK-tide vs MgATP indicates that FAK1 operates via a sequential kinetic mechanism. Fitting of the initial velocity data to eq 2 resulted in the kinetic parameters in Table 1. The turnover number for FAK1 using FAK-tide as substrate was very small ($k_{cat} = 0.052 \pm 0.001\ s^{-1}$), indeed, significantly smaller than the turnover numbers of other protein kinases using peptide substrates of similar size [Csk, $k_{cat} = 0.8\ s^{-1}$ (*10*); S6K1, $k_{cat} = 0.2\ s^{-1}$ (*23*); PDK1, $k_{cat} = 0.4\ s^{-1}$ (*24*); and AKT, $k_{cat} = 0.4\ s^{-1}$ (*25*)]. The values of the Michaelis and dissociation constants for both substrates were equal within experimental error; that is, $K_{MgATP} = 1.2 \pm 0.1\ \mu M$, $K_{iMgATP} = 1.3 \pm 0.2\ \mu M$ and $K_{FAK\text{-}tide} = 5.6 \pm 0.4\ \mu M$, $K_{iFAK\text{-}tide} = 6.1 \pm 1.1\ \mu M$. This equality would be expected for an enzyme for which catalysis is rate-limiting and suggests a rapid-equilibrium random mechanism. Values for $k_{cat}/K_{MgATP}$ and $k_{cat}/K_{FAK\text{-}tide}$ of $4.3 \times 10^4\ M^{-1}\ s^{-1}$ and $9.3 \times 10^3\ M^{-1}\ s^{-1}$ (Table 1), respectively, also reflect the modest catalytic properties of FAK1. The curvature observed in the plot in Figure 1 at 0.08 and 0.16 $\mu$M MgATP and at the two lowest concentrations of FAK-tide is most likely due to experimental error, as the signal/background at these lowest concentrations was minimal. The apparent curvilinear nature of the initial velocity plot could also result from a steady-state random bi bi mechanism, although if this were the case, one expects to observe similar curvature in double-reciprocal plots for either substrate in

Table 1: Kinetic Parameters from Initial Velocity Studies

| | apparent kinetic parameters | | | | | | |
|---|---|---|---|---|---|---|---|
| varied substrate | $K_{MgATP}$ ($\mu$M) | $K_{iMgATP}$ ($\mu$M) | $k_{cat}/K_{MgATP}$ ($M^{-1}\ s^{-1}$) | $K_{FAK\text{-}tide}$ ($\mu$M) | $K_{iFAK\text{-}tide}$ ($\mu$M) | $k_{cat}/K_{FAK\text{-}tide}$ ($M^{-1}\ s^{-1}$) | $k_{cat}$ ($s^{-1}$) |
| MgATP | | | | | | | |
| FAK-tide | $1.2 \pm 0.1$ | $1.3 \pm 0.2$ | $(4.3 \pm 0.4) \times 10^4$ | $5.6 \pm 0.4$ | $6.1 \pm 1.1$ | $(9.3 \pm 0.7) \times 10^3$ | $0.052 \pm 0.001$ |

Table 2: Dead-End and Product Inhibition Patterns of FAK1

| inhibition pattern | fixed substrate | pattern type | $K_{is}$[a] ($\mu$M) | $K_{ii}$[b] ($\mu$M) | $K_m$[c] ($\mu$M) |
|---|---|---|---|---|---|
| AMP-PNP vs MgATP | peptide, 5 $\mu$M | C[d] | 4.5 ± 0.4 | | 1.0 ± 0.1 |
| AMP-PNP vs peptide | MgATP, 2 $\mu$M | NC[e] | 12 ± 4 | 12 ± 1 | 5.2 ± 0.4 |
| Phe/Tyr-FAK-tide vs MgATP | peptide, 5 $\mu$M | NC | 900 ± 300 | 700 ± 100 | 1.2 ± 0.1 |
| Phe/Tyr-FAK-tide vs peptide | MgATP, 2 $\mu$M | C | 700 ± 100 | | 7.4 ± 0.3 |
| MgADP vs MgATP | peptide, 5 $\mu$M | C | 1.4 ± 0.1 | | 1.2 ± 0.04 |
| MgADP vs peptide | MgATP, 2 $\mu$M | NC | 6.3 ± 3.0 | 4.3 ± 0.5 | 5.3 ± 0.3 |
| P-FAK-tide vs MgATP | peptide, 5 $\mu$M | NC | 530 ± 180 | 640 ± 100 | 1.2 ± 0.1 |
| P-FAK-tide vs peptide | MgATP, 2 $\mu$M | C | 220 ± 20 | | 2.6 ± 0.2 |

[a]Apparent slope inhibition constant. [b]Apparent intercept inhibition constant. [c]Michaelis constant for the varied substrate. [d]Denotes competitive inhibition. [e]Denotes noncompetitive inhibition.

the product and dead-end inhibition data, which was not observed (Figures 2S and 3S in Supporting Information). Data in Figure 1 could not be successfully fitted to an initial velocity expression for a steady-state random mechanism ($v = [(aB + cB^2)A + bBA^2]/[d + fB + hB^2 + (e + jB + mB^2)A + (g + kB)A^2]$, where $a-m$ are collections of kinetic parameters (*26*)). From all considerations above, we conclude that FAK1 does not operate via a steady-state random mechanism.

*Product and Dead-End Inhibition Studies*. The results of product inhibition and dead-end inhibition experiments are shown in Table 2 (more details in Supporting Information Table 2S and Figures 2S and 3S). MgADP is a competitive inhibitor vs MgATP ($K_{is}$ = 1.4 ± 0.1 $\mu$M) and noncompetitive vs FAK-tide. Phospho-FAK-tide is a noncompetitive inhibitor vs MgATP and competitive vs FAK-tide ($K_{is}$ = 220 ± 20 $\mu$M). These product inhibition patterns are consistent with either a Theorell−Chance mechanism or a random bi bi mechanism for which the observed noncompetitive patterns of P-FAK-tide vs MgATP and MgADP vs FAK-tide indicate the formation of the two possible substrate−product dead-end complexes, E-MgADP-FAK-tide (EBQ) and E-MgATP-P-FAK-tide (EAP). From the dead-end inhibition patterns, however, AMP-PNP is a competitive inhibitor of MgATP ($K_{is}$ = 4.5 ± 0.4 $\mu$M) and a noncompetitive inhibitor vs FAK-tide (Table 2). The phenylalanine-substituted peptide analogue of FAK-tide, Phe/Tyr-FAK-tide, exhibited noncompetitive inhibition vs MgATP and competitive inhibition vs FAK-tide ($K_{is}$ = 700 ± 100 $\mu$M) (Table 2). These dead-end inhibition patterns are most consistent with a random bi bi mechanism and rule out a Theorell−Chance mechanism for which an uncompetitive inhibition would be expected for AMP-PNP vs FAK-tide if MgATP were the second substrate to bind.

The apparent values of $K_{is}$ obtained from the competitive inhibition patterns of Table 2 correspond to the true inhibition constants for the respective binding of AMP-PNP and Phe/Tyr-FAK-tide to free enzyme ($K_{iAMP\text{-}PNP}$ = 4.5 ± 0.4 $\mu$M and $K_{iPhe/Tyr\text{-}FAK\text{-}tide}$ = 700 ± 100 $\mu$M). In the case of a rapid-equilibrium random bi bi mechanism, these $K_i$ values may also be afforded by the apparent $K_{is}$ and $K_{ii}$ values of the two noncompetitive inhibition patterns, which provides a useful validation of the kinetic mechanism. For the AMP-PNP vs FAK-tide pattern, $K_{iAMP\text{-}PNP} = K_{is}/(1 + [MgATP]/K_{iMgATP}) = K_{ii}/(1 + [MgATP]/K_{MgATP})$, from which we may obtain respective values of $K_{iAMP\text{-}PNP}$ = 5 ± 3 $\mu$M and 4.7 ± 0.8 $\mu$M, which is in excellent agreement with the inhibition constant obtained from the competitive inhibition data ($K_{iAMP\text{-}PNP}$ = 4.5 ± 0.4 $\mu$M). From the noncompetitive dead-end inhibition data of Phe/Tyr-FAK-tide vs MgATP, $K_{iPhe/Tyr\text{-}FAK\text{-}tide} = K_{is}/(1 + [FAK\text{-}tide]/K_{iFAK\text{-}tide}) = K_{ii}/(1 + [FAK\text{-}tide]/K_{FAK\text{-}tide})$, from which one may solve respective values of $K_{iPhe/Tyr\text{-}FAK\text{-}tide}$ = 500 ± 300 $\mu$M and 400 ± 100 $\mu$M, which are in reasonable agreement with the value $K_{iPhe/Tyr\text{-}FAK\text{-}tide}$ = 700 ± 100 $\mu$M obtained from the competitive inhibition data for the peptide inhibitor.

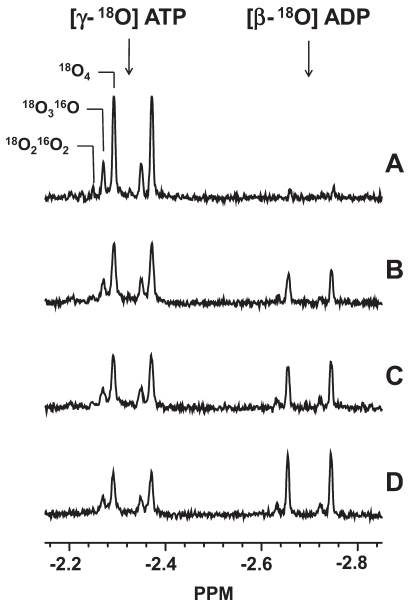


FIGURE 2: $^{31}P$ NMR spectra at 242.76 MHz of [$\gamma$-$^{18}O$]ATP and [$\beta$-$^{18}O$]ADP for various incubation times of FAK-catalyzed positional isotope exchange as outlined in Table 3. The chemical shifts are relative to an external sample of 85% $H_3PO_4$/15% $D_2O$ measured in a separate tube. (A) Experiment 1: [$\gamma$-$^{18}O$]ATP under assay buffer conditions in the absence of FAK. The number of atoms of $^{18}O$ in each of the peaks of a doublet of the $\gamma$-phosphorus group is noted. (B−D) Experiments 2−4: FAK-catalyzed positional isotope exchange of [$\gamma$-$^{18}O$]ATP for incubation times of 73, 146, and 249 min, respectively. A pair of doublets corresponding to the [$\beta$-$^{18}O$]ADP formed in the reaction is seen upfield from the $\gamma$-phosphorus resonances. Additional details are provided in Table 3 and in the text.

The dead-end substrate−product complexes E-MgADP-FAK-tide (EBQ) and E-MgATP-phospho-FAK-tide (EAP) must form to account for the noncompetitive product inhibition patterns observed. The formation of the MgATP-P-FAK-tide (EAP) complex is surprising, because intuitively one would expect untoward steric interactions between the $\gamma$-phosphate of MgATP and the phosphorylated peptide in the active site. It is unlikely that this dead-end complex has physiological significance. Despite this, E-MgATP-phosphocreatine and E-MgADP-creatine complexes have precedence in creatine kinase (*27*). The E-MgADP-peptide (EBQ) complex has been observed for other kinases, specifically for the E-MgADP-Ser-peptide complex of

Table 3: Positional Isotope Exchange of [$\gamma$-$^{18}$O]ATP Catalyzed by Human FAK[a]

| expt | incubation time (min) | % of [$\gamma$-$^{18}O_4$]ATP[b] | % of [$\gamma$-$^{18}O_3{}^{16}$O]ATP[b] | fraction of exchange reaction ($F_x$)[c] | fraction of catalytic reaction ($F_{cat}$)[d] | rate of MgATP exchange ($v_{ex}$) ($\mu$M/s)[e] | rate of MgADP formation ($v_{cat}$) $\mu$M/s)[f] | $k_x/k_{cat}$[g] |
|---|---|---|---|---|---|---|---|---|
| 1 | 0 | 74.4 | 25.6 | 0.0 | 0.0 | 0.0 | 0.0 | 0.0 |
| 2 | 73 | 72.8 | 27.2 | 0.040 | 0.25 | 0.0082 | 0.056 | 0.15 |
| 3 | 146 | 72.3 | 27.7 | 0.052 | 0.35 | 0.005 | 0.04 | 0.12 |
| 4 | 249 | 71.1 | 28.9 | 0.080 | 0.47 | 0.0037 | 0.027 | 0.14 |
| | | | | | | | | $0.14 \pm 0.01$ |

[a] 40 mM HEPES (pH 7.2), 10 mM $MgCl_2$, 1 mM DTT, 1 mM [$\gamma$-$^{18}$O]ATP, 1.5 mM FAK-tide, and 100 nM FAK ($21 \pm 1$ °C). For expt 2−4, quantification of MgADP concentrations as determined by coupled enzyme assay indicated fractions of catalysis of 0.25, 0.41, and 0.56, respectively. [b] Sums of peak intensities of data in Figure 2. [c] Fraction of [$\gamma$-$^{18}$O]ATP exchanged; $F_x = ([\gamma\text{-}^{18}O_4]_t - [\gamma\text{-}^{18}O_4]_0)/([\gamma\text{-}^{18}O_4]_0 - [\gamma\text{-}^{18}O_4]_{eq})$, where $[\gamma\text{-}^{18}O_4]_0$ and $[\gamma\text{-}^{18}O_4]_{eq}$ = 74.4% and 24.8%, respectively. [d] Sums of $\beta$-phosphate peak intensities/total $\beta$- and $\gamma$-phosphate peak intensities, which were corrected for MgADP (7%) in the [$\gamma$-$^{18}$O]ATP sample. [e] Determined from the method of Litwin and Wimmer (*47*), wherein $v_{ex} = [X/\ln(1 - X)](ATP_0/t)[\ln(1 - F_x)]$ wherein $X = F_{cat}$, t = reaction time, and $ATP_0 = 1000$ $\mu$M. [f] Determined from ratios of peak intensities of sums of $\beta$-phosphate peaks divided by total peak intensities of $\gamma$- and $\beta$-phosphate signals. [g] $v_{ex}/v_{cat}$.

the cAMP-dependent protein kinase (*28*). From the apparent product inhibition constants in Table 2, the equilibrium constants describing the formation of the [E-MgATP][P-FAK-tide]/[E-MgATP-P-FAK-tide] and [E-MgADP][FAK-tide]/[E-MgADP-FAK-tide] complexes are respectively $K_{Iap} = 190 \pm 60$ $\mu$M and $K_{Ibq} = 1.6 \pm 0.2$ $\mu$M (Table 1S in Supporting Information). The E-MgATP-P-FAK-tide complex is therefore 100-fold less stable than the E-MgADP-FAK-tide complex, and moreover, the E-MgADP-FAK-tide is slightly more stable than the E-MgADP complex ($K_{iq} = 2.5 \pm 1.0$ $\mu$M). This latter result demonstrates the relative stability of the ternary E-MgADP-FAK-tide complex compared to E-MgADP.

*Positional Isotope Exchange of [$\gamma$-$^{18}O_4$]ATP*. The ability of FAK1 to catalyze $\beta\gamma$-bridge:$\beta$-nonbridge positional oxygen exchange (*29*) of [$\gamma$-$^{18}$O]ATP would provide kinetic information about the partitioning of the E-MgADP-P-FAK-tide ternary complex to either form products or to regenerate its MgATP and FAK-tide substrates. FAK1-catalyzed PIX of [$\gamma$-$^{18}$O]ATP was determined at saturating concentrations of both substrates and analyzed by $^{31}$P NMR using the method of Cohn and Hu (*16*). PIX would be evident by the progressive enrichment of the peak intensity of the [$\gamma$-$^{18}O_3{}^{16}$O]ATP species at the "expense" of the parent [$\gamma$-$^{18}O_4$]ATP species, which arises as a result of the scrambling of the single $\beta\gamma$-bridge $^{18}$O atom into the nonbridge position of the $\beta$-phosphate of the enzyme-bound [$\beta$-$^{18}$O]-MgADP prior to the re-formation of [$\gamma$-$^{18}$O]ATP.

From $^{31}$P NMR spectra, the substitution pattern of $^{18}$O atoms in the $\gamma$-phosphate of the synthetic [$^{18}$O]ATP was found to be $\gamma$-$^{18}O_4$, 74.4%, and $^{8}O_3{}^{16}$O, 25.6% (Figure 2, Table 3). As shown in Figure 2, FAK1 catalyzes the time-dependent decrease and increase, respectively, of the [$\gamma$-$^{18}O_4$]ATP and [$^{18}O_3{}^{16}$O]ATP forms, indicating that PIX has occurred. A tabulation of these data is found in Table 3. The rate of PIX of [$\gamma$-$^{18}O_4$]ATP is 12−15% of the rate of MgATP hydrolysis throughout the time course of the study, and this ratio of rates of exchange to catalysis is invariant as the reaction progresses (average of $k_x/k_{cat} = 0.14 \pm 0.01$), although the rates of exchange ($v_{ex}$) and catalysis ($v_{cat}$) both decrease as reaction times are elongated. The observed PIX most likely arises from the reverse of the E-MgADP-P-FAK-tide complex to substrates rather than the re-formation of exchanged MgATP from the dissociated MgADP and P-FAK-tide products. This is evident from two observations: (1) under the experimental conditions of PIX, the ratio of the rate of the reverse:forward reactions, found to be 0.048,[2] was far lower than the average value of $k_x/k_{cat} = 0.14 \pm 0.01$, and (2) the formation of the dead-end E-MgADP-P-FAK-tide complex, which contributes to the observed diminution of values of $v_{ex}$ and $v_{cat}$ as the MgADP product accumulates ($F_{cat} > 0.25$), would further retard, if not ablate, the formation of MgATP from MgADP and P-FAK-tide. The value of $k_x/k_{cat}$ demonstrates that the regeneration of ATP from the E-MgADP-P-FAK-tide enzyme form occurs 14% as frequently as the formation of MgADP product. This indicates that despite the low value of $k_{cat}$, the ability of the E-MgADP-P-FAK-tide complex to re-form substrates suggests that a slow step follows the formation of this ternary enzyme−product complex and that the phosphoryl group transfer reaction is reversible.

*Effects of Viscosogens on the Steady-State Kinetic Parameters*. The steady-state kinetic parameters for FAK1-catalyzed phosphorylation of FAK-tide were measured in buffers of varying relative viscosity ($\eta_{rel} = 1.0-3.8$). It is expected that increasing concentrations of a microviscogenic agent, such as sucrose, will diminish the rate constants, specifically, if the substrate-binding steps, product-release steps, or a protein conformational change that is affected by solvent, comprises slow kinetic steps in the respective $k_{cat}/K_m$ or $k_{cat}$ expressions (*30*). However, if phosphoryl group transfer is the sole rate-determining step, then no viscosity effects would be expected (*30*, *31*). Macroviscogenic agents, such as Ficoll 400, affect the viscosity of the solution without altering small molecule diffusional rates (*32*), such that viscosity effects arising from sucrose, but not Ficoll 400, would result from changes to the diffusional rates of substrates and products.

Shown in Figure 3 are the initial velocity curves for variable FAK-tide at fixed saturating MgATP (10 $\mu$M). It is evident that $k_{cat}$ decreases as sucrose concentration increases and that this effect is not observed at the highest concentration of Ficoll 400 (10%), despite its higher relative viscosity than 40% sucrose. From initial velocity data for each substrate at changing-fixed concentrations of sucrose, replots of the apparent values of $k_{cat}$ vs relative viscosity ($\eta_{rel}$) for either substrate and $k_{cat}/K_{MgATP}$ were linear with a negative slope, while the plot of $k_{cat}/K_{FAK\text{-}tide}$ vs $\eta_{rel}$

[2] By use of the two coupled-enzyme systems, we compared in separate reaction mixtures the FAK1-catalyzed production of MgATP from 500 $\mu$M MgADP and 500 $\mu$M phospho-FAK-tide and MgADP from 1000 $\mu$M MgATP and 1500 $\mu$M FAK-tide with 100 nM FAK1 (40 mM HEPES (pH 7.2), 10 mM $MgCl_2$, 3 mM DTT, $21 \pm 1$ °C, 50−120 min incubation). Under these conditions, the ratio of the initial rate of the reverse reaction was much less than that of the forward reaction ($v_{rev}/v_{for} = 0.048$).

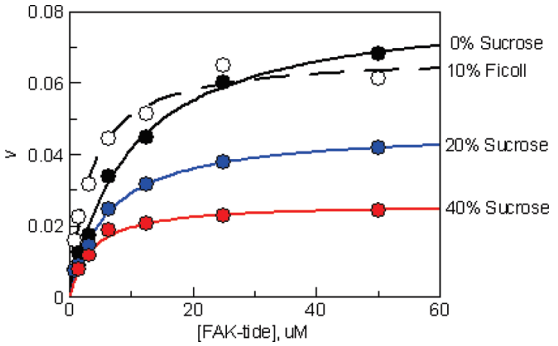


FIGURE 3: Effect of increasing viscosity (both microscopic and macroscopic) on the FAK-catalyzed reaction at 12 $\mu$M MgATP conditions. Data are from fits of initial velocity data to eq 1, where v is in picomoles of product per minute.

had an apparent slope of zero (data not shown). As expected, values of $k_{cat}$ and $k_{cat}/K_m$ for either substrate were not affected by increasing concentrations of the macroviscogen Ficoll 400. The linear diminution in values of $k_{cat}$ and $k_{cat}/K_{MgATP}$, which were not observed for $k_{cat}/K_{FAK\text{-}tide}$, indicated that the kinetic steps involving the binding of MgATP, but not FAK-tide, and one or more postcatalytic steps are affected by solvent viscosity.

Further analysis of the viscosity dependence of these initial velocity data in double-reciprocal form, that is, a plot of 1/v vs 1/MgATP at changing-fixed values of $\eta_{rel}$, conformed to an intersecting pattern as both slope and intercept effects were observed as values of $\eta_{rel}$ were increased (Figure 4A). Fitting of the data in Figure 4A to eq 5 resulted in a slope factor of $k_a = 0.036 \pm 0.003\ \mu M^{-1}\ s^{-1}$ and two intercept factors of $k_c = 0.05 \pm 0.01\ s^{-1}$ and $k_d = 0.08 \pm 0.02\ s^{-1}$. The plot of 1/v vs 1/FAK-tide at changing-fixed values of $\eta_{rel}$ conformed to an apparent parallel pattern for which an intercept effect was observed as values of $\eta_{rel}$ were increased (Figure 4B). From fitting of these data to eq 6, two slope factors of $k_a = 40 \pm 20\ mM^{-1}\ s^{-1}$ and $k_b = 0.4 \pm 1\ \mu M^{-1}\ s^{-1}$ and two intercept factors of $k_c = 0.2 \pm 0.1\ s^{-1}$ and $k_d = 0.083 \pm 0.007\ s^{-1}$ were obtained. That the values of $k_d$ in both plots are equal suggests that the viscosogen exerts an equivalent effect on one or more rate constants within the expression for $k_{cat}$. Also, the lack of an apparent slope effect from the changing-fixed levels of the viscosogen on the plot of 1/v vs 1/FAK-tide reflects the small, and poorly determined, value of the viscosity-dependent term $k_b$, which is obscured by the viscosity-independent slope factor, $k_a$. Combined, these data show that solvent viscosity had no effect on $k_{cat}/K_{FAK\text{-}tide}$, while $k_{cat}$ and $k_{cat}/K_{MgATP}$ were both decreased linearly at increasing solvent viscosity. From the PIX and viscosity data, it may be concluded that enzyme turnover ($k_{cat}$) is rate-limited by both reversible phosphoryl group transfer and a slow step that follows phosphoryl group transfer but precedes product release.

*The Crystal Structure of AMP-PNP-Complexed FAK1.* We have determined the crystal structure of the catalytic domain of active, phosphorylated human FAK1 from crystals grown from FAK1 incubated with AMP-PNP. Crystallographic data are shown in Table 4 and details summarized in the Supporting Information section. As shown in Figure 5A, there are two kinase domains of phosphorylated FAK1/AMP-PNP binary complex molecules in the asymmetric unit. Overall, as observed previously for the FAK1-ADP complex (*19*), the FAK1 catalytic core has the typical bilobal kinase fold (*33*, *34*), comprised of an N-terminal lobe (residues 414−500) formed by a $\beta$-sheet and single α-helix, helix C, and a C-terminal α-helical lobe domain (residues 506−686) (Figure 5A, Supporting Information

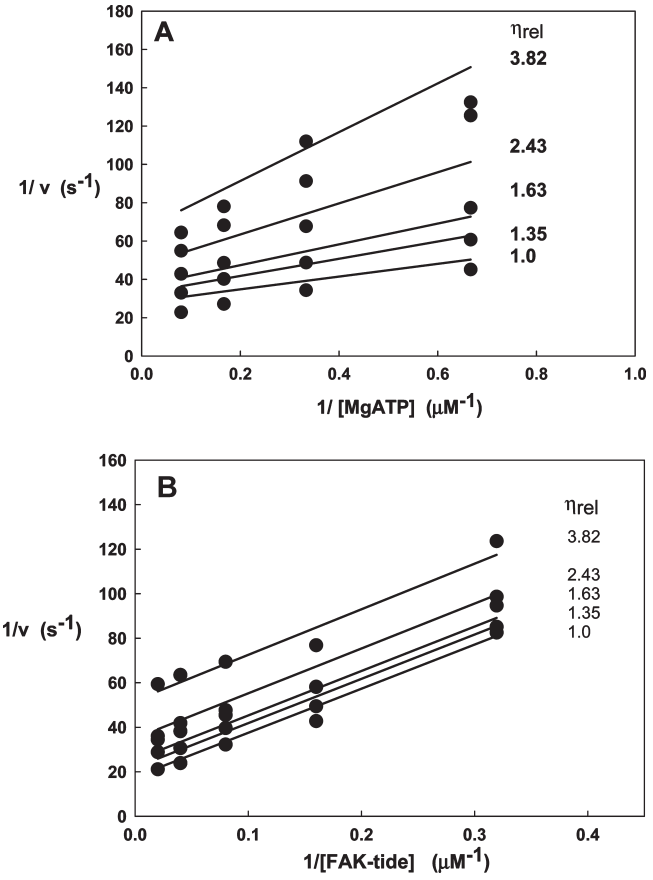


FIGURE 4: (A) Double-reciprocal plot of initial velocity data of FAK with changing fixed levels of sucrose (0−40%; $\eta_{rel}$ = 1.0−3.8), variable concentrations of MgATP (0.1−12 $\mu$M), and 25 $\mu$M FAK-tide. The lines drawn through the experimental data points were fitted to eq 5. (B) Double-reciprocal plot of initial velocity data of FAK with changing fixed levels of sucrose (0−40%; $\eta_{rel}$ = 1.0−3.8), variable concentrations of FAK-tide (0.39−50 $\mu$M), and 12 $\mu$M MgATP. The lines drawn through the experimental data points were fitted to eq 6.

Table 2S). The two molecules interact mostly via two identical loop regions (440−450) that comprise essential parts of both active sites. The active site is situated at the interface between the lobes and includes the ATP (AMP-PNP) binding site and the kinase activation loop segment (residues 564−584; Figure 5B). The AMP-PNP is clearly identified by electron density in the ATP-binding pocket and interacts with the protein both directly and through water-mediated contacts,[3] although the $\gamma$-phosphate group is not evident (Supporting Information Table 2S). The α- and $\beta$-phosphates of AMP-PNP interact with the activation loop residues Lys581 (2.7 Å to O2A) and Lys 583 (2.7 Å to N3B).

Comparison of this AMP-PNP-FAK1-complexed structure to the published structures of inactive, unphosphorylated FAK1 (*5*, *19*) reveals one significant conformational difference. As shown in the AMP-PNP-complexed structure in Figure 5B, the activation loop is mostly ordered, with residues visibly interacting with the α- and $\beta$-phosphates of AMP-PNP (amino acids 564−584), and apparently covers the ATP-binding site. However, the activation loop in the inactive FAK1 structure is oriented away from the ATP-binding site and is essentially part of

[3]Crystallography details about the AMP-PNP-FAK1 interactions are summarized in the Supporting Information section.

Table 4: Data Collection and Refinement Statistics for Crystallographic Data for the Kinase Domain of Focal Adhesion Kinase-1 (411−686) in Complex with AMP-PNP

| | |
|---|---|
| **Data Collection** | |
| space group | $P2_1$ |
| cell dimensions | |
| *a*, *b*, *c* (Å) | 39.7, 176.8, 39.8 |
| α, *β*, *γ* (deg) | 90.0, 107.9, 90.0 |
| resolution (Å) (last shell) | 1.45 (1.51−1.45) |
| $R_{sym}$[a] (last shell) | 0.049 (0.287) |
| $I/\sigma_I$ (last shell) | 31.0 (2.53) |
| completeness (%) (last shell) | 86.4 (53.0) |
| redundancy (last shell) | 3.3 (2.6) |
| **Refinement** | |
| resolution (Å) | 25−1.45 |
| no. of reflections | 72951 |
| $R_{work}$[b]/$R_{free}$[c] | 0.231/0.241 |
| no. of atoms | |
| protein | 4204 |
| ligand | 54 |
| water/solvent | 206 |
| *B*-factors | |
| protein | 23.9 |
| ligand | 52.2 |
| water/solvent | 53.1 |
| rms deviations | |
| bond lengths (Å) | 0.005 |
| bond angles (deg) | 0.878 |

the C-terminal α-helical lobe domain, leaving the ATP-binding site open to solvent. Interestingly, only one major conformational change, that of the activation loop, has been observed for FAK1. The structural analyses of most protein kinases (*35*) have identified two major conformational changes upon ATP binding: the activation loop movement as seen for FAK1 and an additional significant conformational change of the C-helix. The movement of the C-helix toward the active site promotes the formation of the salt bridge between the active site residues Lys454 and Glu471 that characterizes the active form of protein kinases. This movement of the C-helix is not observed in FAK1 structures; the C-helix conformation of FAK1 structures remains unchanged (*5*). This suggests that the conformational change undergone by the activation loop, presumably upon ligand binding, is the major conformation change to be expected during the catalytic cycle of the isolated FAK1 kinase domain. It is tempting to speculate that this single conformational change which attends the binding of MgATP, without a conformational contribution from the C-helix, is reflected in the viscosity dependence of MgATP binding but lack of same with the larger FAK-tide substrate. Furthermore, movement of the C-helix in other protein kinases which employ ordered mechanisms may help to elaborate a peptide binding site in the E-MgATP form and thereby militate an ordered kinetic mechanism. Also of note in the AMP-PNP-complexed structure reported here is that although the protein is phosphorylated (data not shown) and fully active, the two phosphorylated tyrosines (Tyr576, Tyr577), along with five residues from 573 to 578 in the activation segment, are disordered and not resolved in our structure, which suggests that phosphorylation alone may not be sufficient for formation of the active, "closed" conformation.

*A Comprehensive Model of FAK1 Catalysis*. A mechanistic model that accounts for the initial velocity, product and dead-end inhibition, PIX, and viscometric studies and is consistent with the structural evidence for activation loop movement is shown in Scheme 1.

The rate constants for the formation and breakdown of all binary complexes are expected to be much more rapid than catalysis, that is, $k_1$, $k_2$, $k_7$, $k_8$, and $k_{19}-k_{27}$ are faster than $k_{13}$. Enzyme forms denoted with an asterisk indicate steps that follow a conformational change resulting in a "closed" activation loop. Closure or reopening of the kinase activation loop (such as EPQ* → EPQ), described by the $k_4$, $k_{12}$, and $k_{15}$ steps in Scheme 1, may be similar in rate to the catalytic steps and are likely to be affected in the presence of the sucrose viscosogen.

Based on the mechanism shown in Scheme 1, expressions for the initial velocity of FAK1 (eq 7), and by using the method of net rate constants (*36*), expressions for Michaelis and dissociation constants of substrates, $k_{cat}$, viscosity effects, and the rates of PIX to turnover were derived below (eq 7−16). It is assumed that all binary enzyme−substrate, enzyme−product, and the two dead-end enzyme−substrate−product complexes are in rapid equilibrium and that the expression for $V/E_t$ is described by three slow kinetic steps $k_{13}$, $k_{14}$, and $k_{15}$ when $k_3$ and $k_{11} \gg k_{12}$, $k_{13}$, $k_{14}$, and $k_{15}$, and $k_{16}$ is negligible:

$$v = VABE_t/(K_{ia*}K_b(1 + P/K_{ip} + Q/K_{iq}) + K_{a*}B(1 + Q/K_{Ibq}) + K_bA(1 + P/K_{Iap}) + AB) \quad (7)$$

for which $V/E_t = k_{13}k_{15}/(k_{13} + k_{14} + k_{15})$, $K_{ia*} = k_2k_4/k_1k_3$, $K_{ib} = k_8/k_7$, $K_{ip} = k_{23}/k_{24}$, $K_{iq} = k_{19}/k_{20}$, $K_{Iap} = k_{26}/k_{25}$, $K_{Ibq} = k_{28}/k_{27}$, and $K_{a*}$ and $K_b$ will be defined below.

The effects of the viscosogen sucrose on the kinetic parameters $k_{cat}$, $k_{cat}/K_{MgATP}$, and $k_{cat}/K_{FAK\text{-}tide}$ were performed at saturating concentrations of the fixed substrate, such that the expression for $k_{cat}/K_{MgATP}$ describes the lower pathway in Scheme 1 (E-FAK-tide combines with MgATP), while $k_{cat}/K_{FAK\text{-}tide}$ describes the upper pathway (E-MgATP* combines with FAK-tide). Expressions for these three kinetic parameters are found in eq 8−10, with the assumptions that $k_{13}$, $k_{14}$, and $k_{15}$ are considerably slower than the steps representing closing of the activation loop ($k_3$ and $k_{11}$) and that the substrate desorption step $k_6$ is much faster than reopening of the activation loop ($k_{12}$ and $k_{15}$) and phosphoryl transfer ($k_{13}$ and $k_{14}$).

$$k_{cat}/K_{MgATP*} = [k_9k_{11}(k_{13}k_{15}/(k_{14} + k_{15}))]/[k_{10}(k_{12} + k_{13}k_{15}/(k_{14} + k_{15})) + k_{11}(k_{13}k_{15}/(k_{14} + k_{15}))] \approx k_9k_{11}/(k_{10} + k_{11}) \quad (8)$$

$$k_{cat}/K_{FAK\text{-}tide} = [k_5(k_{12} + k_{13}k_{15}/(k_{14} + k_{15}))(k_3/k_4)]/([k_6 + k_{12} + k_{13}k_{15}/(k_{14} + k_{15})](1 + k_3/k_4)) \approx (k_3k_5/k_4)/[(k_6(k_{14} + k_{15})/k_{13}k_{15} + 1)(1 + k_3/k_4)] \quad (9)$$

$$k_{cat} = 1/[1/k_3 + 1/k_{11} + (k_{14} + k_{15})/k_{13}k_{15} + 1/k_{15}] \approx k_{13}k_{15}/(k_{13} + k_{14} + k_{15}) \quad (10)$$

As one expects that the viscosogen will lower the rates of substrate binding, product desorption steps, and, possibly, conformational movements of the activation loop by the amount of relative viscosity (for example, $k_9^o = k_9/\eta_{rel}$, where $k_9$ is the rate constant at no viscosogen), the expressions for the effect of sucrose on the three kinetic parameters in eq 8−10 are found in eq 11−13.

$$k_{cat}/K_{MgATP*(\eta_{rel})} = k_9k_{11}/(k_{10} + k_{11})\eta_{rel} \quad (11)$$

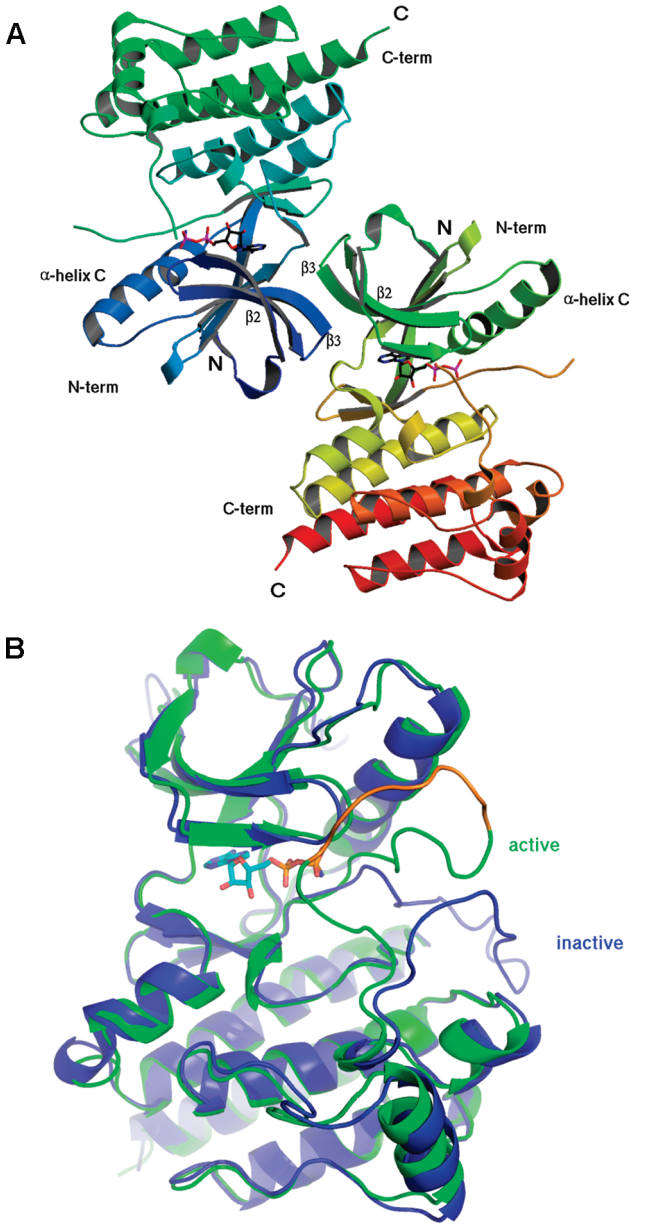


FIGURE 5: (A) Crystal structure of the kinase domain of human focal adhesion kinase (chain A, amino acids 414−686; chain B, amino acids 415−686) in complex with AMP-PNP. The N-terminal lobe is formed by residues 414−500 and the C-terminal lobe by residues 506−686. The two independent molecules interact mainly through residues 448−450 in $\beta$-strands 3. (B) Structural overlay of inactive, unphosphorylated FAK1 (2J0J) and active, phosphorylated FAK1. The activation segment in the active, AMP-PNP complex is close to the N-lobe and covers the ATP-binding site while in the inactive, unphosphorylated FAK1 the activation loop is removed from the active site. Colored orange is the modeled trajectory of the section of the activation loop not seen in the structure.

$$k_{cat}/K_{FAK\text{-}tide(\eta_{rel})} = (k_3k_5/k_4)/[(k_6(k_{14}\eta_{rel} + k_{15})/k_{13}k_{15} + 1)(1 + k_3/k_4)] \quad (12)$$

$$k_{cat(\eta_{rel})} = k_{13}k_{15}/[(k_{13} + k_{14})\eta_{rel} + k_{15}] \quad (13)$$

Accordingly, the parameters $k_a-k_d$ obtained from fitting of the double-reciprocal data in Figure 4 to either eq 5 or eq 6 may now be related to the individual rate constants of Scheme 1 and in eq 11−13. From the double-reciprocal analysis of viscosity effects on variable MgATP (Figure 4A), the value of $k_a = k_9k_{11}/(k_{10} + k_{11}) = 0.036 \pm 0.003\ \mu M^{-1}\ s^{-1}$ was similar to the apparent value of $k_{cat}/K_{MgATP*} = 0.04 \pm 0.01\ \mu M^{-1}\ s^{-1}$ (at [sucrose] = 0). It is noteworthy that if the expression for $k_{cat}/K_{MgATP*}$ found in eq 8 was merely the reciprocal of the dissociation constant for MgATP binding to E-FAK-tide ($k_9/k_{10}$), there would be no effect of viscosity on this expression as sucrose would be expected to lower values of both $k_9$ and $k_{10}$ equally. The observed slope effects seen in Figure 4A likely arise because of the additional effect of the viscosogen on the closing of the activation loop as described by $k_{11}$, giving rise to the expression in eq 11. The resulting values of $k_c = k_{13} = 0.05 \pm 0.01\ s^{-1}$ and $k_d = k_{13}k_{15}/(k_{13} + k_{14}) = 0.08 \pm 0.01\ s^{-1}$ reflect low values of the rate constants of trans-phosphorylation and opening of the activation loop following catalysis.

The plot of 1/v vs 1/FAK-tide at changing-fixed values of $\eta_{rel}$ conformed to an apparent parallel pattern for which an intercept effect was observed as values of $\eta_{rel}$ were increased (Figure 4B). For FAK-tide, a higher value for $k_c = k_{13} = 0.2 \pm 0.1\ s^{-1}$ was obtained, with the same value found for $k_d = k_{13}k_{15}/(k_{13} + k_{14}) = 0.083 \pm 0.007\ s^{-1}$. The parameter $k_a = k_6/k_5k_{13} = K_{ib}/k_{13} = 40 \pm 20\ \mu M^{-1}\ s^{-1}$, which from the experimental value of $K_{ib} = 6.1 \pm 1.1\ \mu M$ from the initial velocity data, upon solution also results in a value of $k_{13} = 0.2\ s^{-1}$. The absence of a slope effect in the plot of 1/v vs 1/FAK-tide arises from the comparatively modest size of the bimolecular rate constant of FAK-tide combining with E-MgATP ($k_b = k_5 = 40000\ M^{-1}\ s^{-1}$) and reflects the small, and poorly determined, value of the viscosity-dependent term, $k_b$.

Importantly, the results of the effects of the viscosogen sucrose on the initial velocity data, while in accord with a random bi bi kinetic mechanism, do not support a kinetic mechanism for which phosphoryl transfer is the sole rate-limiting step in catalysis. This is because changes in solvent viscosity are not expected to affect the rates of binding and desorption for substrates and products that are in true rapid equilibrium with the enzyme. That is, for kinetic events that are far more rapid than the rate of phosphoryl transfer, the observation of significant viscosogenic effects on both $k_{cat}$ and $k_{cat}/K_{MgATP}$ indicates that one or more steps involved in the binding of MgATP or a postbinding conformational change and product release are slow enough to influence the values of these kinetic parameters under the assumption that catalysis is also very slow.

The observation of FAK1-catalyzed PIX of [$\gamma$-$^{18}$O]ATP is also consistent with the lack of a purely rapid-equilibrium mechanism, since a rapid release of [$\beta$-$^{18}$O]ADP from the E-MgADP-P-FAK-tide complex would not support the re-formation of scrambled [$\gamma$-$^{18}$O]ATP by facile reversal of this complex. From Scheme 1, one may write an expression for the ratio of the rate of PIX to turnover by the use of the method of net rate constants (*36*) in order to integrate these data with the outcome of the viscosity effect data to provide solutions for the rate constants $k_{13}$, $k_{14}$, and $k_{15}$:

$$\begin{aligned} k_x/k_{cat} &= k_{14}'/k_{15}' \\ &= k_{14}k_{12}k_{10}/[(k_{10}(k_{12} + k_{13}) + k_{11}k_{13})k_{15}] \\ &= (k_{14}/k_{15})/[1 + (k_{13}/k_{12})(1 + k_{11}/k_{10})] \\ &\approx (k_{14}/k_{15})/[1 + (k_{13}/k_{12})] \end{aligned} \quad (14)$$

We assume that $k_{10} > k_{11}$ and that $k_{12} \approx k_{15}$ as both steps comprise the opening of the activation loop from the respective E-MgATP-FAK-tide and E-MgADP-P-FAK-tide complexes.

From the average experimental value of $k_x/k_{cat} = (k_{14}/k_{15})/[1 + (k_{13}/k_{12})] = 0.14 \pm 0.01$, wherein $k_{12} \approx k_{15}$, and from kinetic

Scheme 1

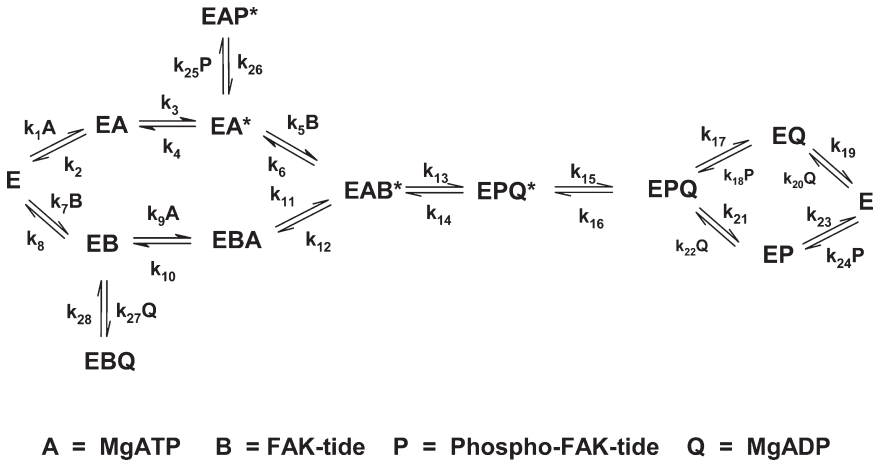


Scheme 2: Kinetics of the Ternary Complexes of FAK1[a]

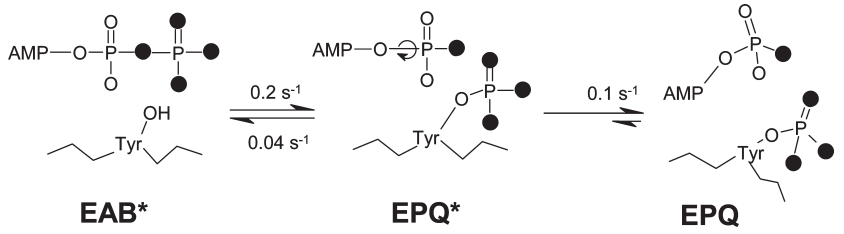


[a]In this scheme, EAB* represents the MgATP-FAK-tide-bound complex with the activation loop "closed", EPQ* represents the MgADP-phospho-FAK-tide-bound complex with the activation loop "closed", and EPQ represents the MgADP-phospho-FAK-tide-bound complex with the activation loop in the "open" confirmation.

constants obtained from the viscosity data for MgATP above ($k_c = k_{13} = 0.05 \pm 0.01\ s^{-1}$ and $k_d = k_{13}k_{15}/(k_{13} + k_{14}) = 0.08 \pm 0.01\ s^{-1}$), we may solve for values of these three rate constants: $k_{13} = 0.05 \pm 0.01\ s^{-1}$, $k_{14} = 0.02 \pm 0.05\ s^{-1}$, and $k_{15} = 0.12 \pm 0.04\ s^{-1}$. By use of eq 14, we may calculate $k_{cat} = 0.03 \pm 0.02\ s^{-1}$, from these three solved rate constants, which compares favorably with the apparent value of $k_{cat} = 0.04 \pm 0.004\ s^{-1}$ obtained from the viscosity data with MgATP above. A similar assessment with values from the viscosity data with FAK-tide where $k_{13} = 0.2 \pm 0.1\ s^{-1}$, $k_{13}k_{15}/(k_{13} + k_{14}) = 0.083 \pm 0.007\ s^{-1}$, and $k_{14}/(k_{13} + k_{15}) = 0.14 \pm 0.01$, we calculate values of $k_{14} = 0.04 \pm 0.04\ s^{-1}$ and $k_{15} = 0.1 \pm 0.01\ s^{-1}$ from which we may obtain $k_{cat} = 0.06 \pm 0.04\ s^{-1}$, from these three solved rate constants, which compares favorably with the apparent value of $k_{cat} = 0.06 \pm 0.001\ s^{-1}$, obtained from the viscosity data with FAK-tide. It is likely that this value of $k_{cat} = 0.06 \pm 0.001\ s^{-1}$ is more reflective of the true $k_{cat}$ of FAK1 because (a) a limiting value of $k_{cat} = 0.052 \pm 0.001\ s^{-1}$ was obtained from the initial velocity data and (b) the changing-fixed level of MgATP ([MgATP] = $10K_{MgATP}$) in this study is a more saturating level than the counterpart value of changing-fixed FAK-tide ([FAK-tide] = $5K_{FAK\text{-}tide}$) in the data of Figure 4A. Accordingly, we propose that the limiting values of the rate constants of $k_{13} = 0.2 \pm 0.1\ s^{-1}$, $k_{14} = 0.04 \pm 0.04\ s^{-1}$, and $k_{15} = 0.1 \pm 0.01\ s^{-1}$ are the more representative from our studies. From this it is evident that phosphoryl transfer is faster in the forward reaction than the reverse reaction and is twice the rate of the postcatalytic reopening of the activation loop. Scheme 2 summarizes the relative rates of the ternary complexes vs the putative conformational change in the $k_{15}$ step determined by the viscosity and PIX experiments.

Normally, one expects that for a purely rapid-equilibrium random bi bi mechanism for which catalysis is completely rate-limiting that Michaelis and dissociation constants for substrates will be identical (*37*), as observed experimentally for FAK1. The availability of solved rate constants for the slow kinetic steps represented by $k_{13}$, $k_{14}$, and $k_{15}$ now allows evaluation of the virtual identity of the Michaelis and dissociation constants of the substrates for FAK1 for which we have demonstrated that the rate of a postcatalytic conformational change step is slower than phosphoryl transfer. The expressions for the Michaelis constants under conditions that the fixed substrate is saturating are found in eqs 15 and 16.

$$K_{MgATP*} = [k_{13}k_{15}/(k_{13} + k_{14} + k_{15})][(k_{10} + k_{11})/k_9k_{11}] = 1.2 \pm 0.1\ \mu M \quad (15)$$

$$K_{FAK\text{-}tide} = [k_6(k_{15} + k_{14})(1 + k_3/k_4)]/[(k_{13} + k_{14} + k_{15})(k_3k_5/k_4)] = 5.4 \pm 0.5\ \mu M \quad (16)$$

These expressions may now be compared with their counterpart substrate dissociation constants of $K_{iMgATP*} = k_2k_4/k_1k_3 = 1.3 \pm 0.2\ \mu M$ and $K_{iFAK\text{-}tide} = k_8/k_7 = 6.1 \pm 1.1\ \mu M$. When $k_{13} > k_{15} > k_{14}$ and $k_{10} > k_{11}$, $K_{MgATP*}$ approximates $k_{10}k_{15}/k_9k_{11}$, which would be equal to $K_{iMgATP*} = k_4k_2/k_3k_1$ when the rate constants for equivalent kinetic steps in the two pathways are all equal ($k_1 = k_9$, $k_2 = k_{10}$, $k_3 = k_{11}$, and $k_4 = k_{12} \sim k_{15}$, as both of these latter rate constants describe opening of the activation loop). In kind, the expression for $K_{FAK\text{-}tide}$ equals $(k_6/k_5)[(k_{14} + k_{15})/(k_{13} + k_{14} + k_{15})]$ when $k_3/k_4 \gg 1$ and $k_{13} > k_{15} > k_{14}$ and will be nearly equal to $K_{iFAK\text{-}tide}$ when $k_5 = k_7$ and $k_6 = k_8$. The

equality of the Michaelis and dissociation constants suggests that the rates of the commensurate kinetic steps in the two branches of the random pathway are also equal.

The internal equilibrium constant of phosphoryl transfer, $K_{int} = k_{13}/k_{14}$ (*38*), of FAK1 may now be calculated to be $0.2 \pm 0.1\ s^{-1}/0.04 \pm 0.04\ s^{-1} = 5 \pm 5$, which is similar to the values of $K_{int} = 1$ obtained for rabbit muscle creatine kinase (*39*) and yeast hexokinase (*40*). By use of the Haldane expression for a rapid-equilibrium random bi bi mechanism ($K_{eq} = V_1K_pK_{iq}/V_2K_{ia*}K_b$ with the approximate ratio[2] of $V_1/V_2 = 20$, and with values of $K_{ip} = 220\ \mu M$ (Supporting Information Table 1S), $K_q \sim K_{iq} = 2.5\ \mu M$ (Table 2 and Supporting Information Table 1S), $K_{ia*} = 1.3\ \mu M$ and $K_b = 5.4\ \mu M$ (Table 1)), one may calculate an equilibrium constant for FAK1 of 1600. The observed disparity between the "internal" and "external" equilibrium constants is found for other kinases, including creatine kinase ($K_{eq} = 0.08$) and hexokinase ($K_{eq} \sim 1000$). The ratio $V_1/V_2 \sim [k_{13}k_{15}(k_{14} + k_{15} + k_{16})]/[k_{14}k_{16}(k_{13} + k_{14} + k_{15})] = 20$ for the values of $k_{13}-k_{15}$ above and when $k_{16} = 0.01$, so that the finding that $K_{eq} \gg K_{int}$ holds for FAK1 when the reopening of the activation loop is far slower than its closing in both directions, such that the substrates are "locked" into the central complexes.

*Mechanistic Implications*. Common to other protein kinases, the binding of MgATP to either free enzyme or E-FAK-tide likely induces a conformational change tantamount to the movement of the activation loop of FAK1 (*31*). It is understood that the activation segment samples a range of conformations that results in the loops being disordered in many instances where the structures have been determined (*32*). It is conceivable that this range of conformations includes an extended conformation away from the active site in a relatively "open" form, as well as a more "closed" conformation that is most often accessed after activation by phosphorylation (*31*) such that, for example, in the case of FAK1, Tyr576 in the activation loop in the presence and absence of the nonhydrolyzable MgATP analogue, AMP-PNP, may traverse as much as 10 Å or more upon binding of the nucleotide analogue. This suggests that this conformational change in the formation of the binary E-MgATP complex is also found in the ternary complex, that is, the binding of MgATP to E-FAK-tide, which is then poised for catalysis. Moreover, it is anticipated that the activation loop must again open ($k_{15} \approx 0.1\ s^{-1}$) to allow the release of the MgADP product from the ternary E-MgADP-phospho-FAK-tide complex. Interestingly, the observation that pTyr575 and pTyr576 and other residues in their vicinity of the activation loop are disordered in the structure of the AMP-PNP- FAK1 complex suggests that phosphorylation of Tyr575 and Tyr576 is not sufficient to promote ordering of the activation loop into a closed conformation; rather, phosphorylation appears to introduce sufficient dynamics into this region of the polypeptide chain that is consistent with it undergoing substantial displacements depending partly on the presence or absence of ligands in the active site.

The kinetic mechanisms utilized by the protein kinases constitute a broad spectrum ranging from fully ordered, where nucleotides are the first and last to bind, to rapid-equilibrium random, as appears to be true for FAK1. Differences in these mechanisms often reflect the range of values of $k_{cat}$ and on the type of substrate used. Kinetics of the C-terminal Src kinase (Csk (*10*)) using a poly(Glu,Tyr) substrate are consistent with a rapid-equilibrium random mechanism. Other findings for Csk were highly similar to FAK1; that is, values of Michaelis and dissociation constants were identical for both substrates, and a postcatalytic step (product release) was slightly slower than the rate of phosphoryl transfer. Both the Cdk5/p25 kinase (*41*) and p21-activated protein kinase (Pak2 (*42*)) have been characterized as rapid-equilibrium random kinetic mechanisms using respectively the *tau* protein and maltose-binding protein (MBP) and an oligopeptide (LIMKtide) as substrates. For Pak2, analysis of kinetic parameters by viscosity effects indicated that for MBP the rate of phosphoryl transfer was twice as fast as desorption of the protein product, giving rise to an effect on $k_{cat}$, while for the LMNtide substrate, no viscosity effect was evident on $k_{cat}$ as product release was 5-fold greater than the rate of catalysis. An important analogue to the FAK1 mechanism is found in the kinetic data of the extracellular-regulated kinase-2 (Erk2 kinase) using the protein substrate Ets(delta)138, for which a solvent viscosity effect is found for both values of $k_{cat}/K_m$ and $k_{cat}$ and from which the authors cite the existence of a random bi bi mechanism which contains a rate-limiting conformational change following substrate binding (*43*).

Through a series of elegant studies, Cook and colleagues have shown that the cAMP-dependent protein kinase operates via a steady-state random mechanism using a serine-containing peptide substrate (*28*), for which isotope partitioning studies revealed that, at high concentrations of $Mg^{2+}$, MgATP and serine-peptide desorb from central complexes more slowly than catalysis (*44*). Interestingly, the kinetic mechanism of the reverse reaction of cAMP-dependent protein kinase was shown to vary with changes of pH, as an equilibrium-ordered mechanism (phosphopeptide binding to free enzyme) at low pH converts to a steady-state random mechanism for which MgADP now preferentially binds first as the pH was raised (*45*).

The random mechanism elucidated herein for FAK1 is concordant with that of other protein kinases that play similarly crucial roles both in phosphorylation of other cellular proteins that induce signal transduction events and by autoactivation via phosphorylation of endogenous sequences within the kinase. The low value of $k_{cat}$ for FAK1 using FAK-tide as substrate undoubtedly contributes to the observed random mechanism in that for the low rate of phosphoryl transfer ($k_{13} = 0.2\ s^{-1}$) the desorption rates of the substrates and products are significantly faster such that the kinetics approximate a rapid-equilibrium model, as reflected in the equality of the Michaelis and dissociation constants. These kinetic findings may have a physiological significance. First, since the FAK-tide substrate is a mimic of the site of autophosphorylation in full-length FAK1, the binding and processing of FAK-tide may be competing with the high local concentration of the analogous, endogenous substrate sequence (phosphorylated or not) within FAK1. This could account for the poor kinetics of the "free" peptide substrate. Second, the random mechanism observed for FAK1 and other protein kinases with poor turnover numbers may constitute a mechanism of substrate fidelity. One would expect that a more rapid, and therefore less selective, rate of phosphorylation of cellular proteins would give rise to adventitious, and possibly catastrophic, signaling pathways. Accordingly, a poor turnover and non-"sticky" substrates, as observed here, guarantee a judicious selection by FAK1 for the appropriate peptide sequence. Such substrate fidelity, coupled with an apparent rapid-equilibrium mechanistic component, is manifest in the remarkable specificity of the T7 DNA polymerase, for which substrate misincorporations result in disastrous genetic consequences (*46*).

The current findings contribute to the idea that protein kinases utilize a spectrum of kinetic mechanisms with a variety of

predominant enzyme forms present during catalysis, thus yielding different transitory enzyme forms to target for inhibitor design. An example would be that if desorption of MgADP from a binary kinase complex were rate-limiting in the mechanism, drug discovery efforts could be well served by seeking to find small molecules that specifically bind to the E-MgADP form in order to further retard the regeneration of fresh, unliganded enzyme. For FAK1, the resolution of the kinetics of activation, catalysis, and product release deduced by this work shows that drug discovery efforts for this or kinetically similar protein kinases could focus on developing inhibitors that "trap" the enzyme in the "locked down" closed form that has ATP or ADP bound.

## ACKNOWLEDGMENT

The authors thank Dr. Richard Gontarek and Dr. Ryan Kruger for thoughtful comments and WuXi AppTec Co., Ltd. (Shanghai, China), for the preparation of [$\gamma$-$^{18}$O]ATP.

## SUPPORTING INFORMATION AVAILABLE

Figures 1S−3S and Tables 1S and 2S showing codon optimization of FAK(411−686), product and dead-end inhibition results, and structural details of FAK1 interactions with AMP-PNP. This material is available free of charge via the Internet at http://pubs.acs.org.

## REFERENCES

1. van Nimwegen, M. J., and van de Water, B. (2007) Focal Adhesion Kinase: A Potential Target in Cancer Therapy. *Biochem. Pharmacol. 73*, 597–609.
2. Schlaepfer, D. D., Hauck, C. R., and Sieg, D. J. (1999) Signaling through Focal Adhesion Kinase. *Prog. Biophys. Mol. Biol. 71*, 435–478.
3. McLean, G. W., Carragher, N. O., Avizienyte, E., Evans, J., Brunton, V. G., and Frame, M. C. (2005) The Role of Focal-Adhesion Kinase in Cancer—A New Therapeutic Opportunity. *Nat. Rev. 5*, 505–515.
4. Kornberg, L. J. (1998) Focal Adhesion Kinase and Its Potential Involvement in Tumor Invasion and Metastasis. *Head Neck 20*, 745–752.
5. Lietha, D., Cai, X., Ceccarelli, D. F. J., Li, Y., Schaller, M. D., and Eck, M. J. (2007) Structural Basis for the Autoinhibition of Focal Adhesion Kinase. *Cell 129*, 1177–1187.
6. Arold, S. T., Hoellerer, M. K., and Noble, M. E. (2002) The Structural Basis of Localization and Signalling by the Focal Adhesion Targetting Domain. *Structure 10*, 319–327.
7. Hayashi, I., Vuori, K., and Liddington, R. C. (2002) The Focal Adhesion Targeting (FAT) Region of Focal Adhesion Kinase Is a Four-Helix Bundle That Binds Paxillin. *Nat. Struct. Biol. 9*, 101–106.
8. Calalb, M. B., Polte, T. R., and Hanks, S. K. (1995) Tyrosine Phosphorylation of Focal Adhesion Kinase at Sites in the Catalytic Domain Regulates Kinase Activity: A Role for Src Family Kinases. *Mol. Cell. Biol. 15*, 954–963.
9. Toutant, M., Costa, A., Studler, J. M., Kadare, G., Carnaud, M., and Girault, J. A. (2002) Alternative Splicing Controls the Mechanisms of FAK Autophosphorylation. *Mol. Cell. Biol. 22*, 7731–7743.
10. Cole, P. A., Burn, P., Takacs, B., and Walsh, C. T. (1994) Evaluation of the Catalytic Mechanism of Recombinant Human Csk (C-terminal Src Kinase) Using Nucleotide Analogs and Viscosity Effects. *J. Biol. Chem. 269*, 30880–30887.
11. Prowse, C. N., Hagopian, J. C., Cobb, M. H., Ahn, N. G., and Lew, J. (2000) Catalytic Reaction Pathway for the Mitogen-Activated Protein Kinase ERK2. *Biochemistry 39*, 6258–6266.
12. Waas, W. F., Rainey, M., Szafranska, A., and Dalby, K. (2003) Two Rate-Limiting Steps in the Kinetic Mechanism of the Serine/Threonine Specific Protein Kinase ERK2: A Case of Fast Phosphorylation Followed by Fast Product Release. *Cell. Mol. Biol. Lett. 8*, 516–518.
13. Moffatt, J. G. (1964) A General Synthesis of Nucleosides-5′ Triosphosphates. *Can. J. Chem. 42*, 599–604.
14. Hackney, D., Stempel, K. E., and Boyer, P. D. (1980) Oxygen-18 Probes of Enzymic Reactions of Phosphate Compounds. *Methods Enzymol. 64*, 60–83.
15. Wehlri, W. E., Verheyden, D. L. M., and Moffatt, J. G. (1965) *J. Am. Chem. Soc. 87*, 2265–2277.
16. Cohn, M., and Hu, A. (1978) Isotopic ($^{18}$O) Shift in $^{31}$P Nuclear Magnetic Resonance Applied to a Study of Enzyme-Catalyzed Phosphate−Phosphate Exchange and Phosphate (Oxygen)−Water Exchange Reactions. *Proc. Natl. Acad. Sci. U.S.A. 75*, 200–203.
17. Meek, T. D., Karsten, W. E., and DeBrosse, C. W. (1987) Carbamoyl-Phosphate Synthetase II of the Mammalian CAD Protein. Kinetic Mechanism and Elucidation of Reaction Intermediates by Positional Isotope Exchange. *Biochemistry 26*, 2584–2593.
18. Otwinowski, Z. M., and Minor, W. (1997) Processing of X-ray Diffraction Data Collected in Oscillation Mode. *Methods Enzymol. 276*, 307–326.
19. Nowakowski, J., Cronin, C. N., McRee, D. E., Knuth, M. W., Nelson, C. G., Pavletich, N. P., Rogers, J., Sang, B. C., Scheibe, D. N., Swanson, R. V., and Thompson, D. A. (2002) Structures of the Cancer-Related Aurora-A, FAK, and EphA2 Protein Kinases from Nanovolume Crystallography. *Structure 10*, 1659–1667.
20. McCoy, A. J. (2007) Solving Structures of Protein Complexes by Molecular Replacement with Phaser. *Acta Crystallogr., Sect. D: Biol. Crystallogr. 63*, 32–41.
21. Emsley, P., and Cowtan, K. (2004) Coot: Model-Building Tools for Molecular Graphics. *Acta Crystallogr. D60*, 2126–2132.
22. Murshudov, G. N., Vagin, A. A., and Dodson, E. J. (1997) Refinement of Macromolecular Structures by the Maximum-Likelihood Method. *Acta Crystallogr. D53*, 240–255.
23. Keshwani, M. K., and Harris, T. K. (2008) Kinetic Mechanism of Fully Activated S6K1 Protein Kinase. *J. Biol. Chem. 283*, 11972–11980.
24. Gao, X., and Harris, T. K. (2006) Steady-State Kinetic Mechanism of PDK1. *J. Biol. Chem. 281*, 21670–21681.
25. Zhang, X., Zhang, S., Yamane, H., Wahl, R., Ali, A., Lofgren, J. A., and Kendall, R. L. (2006) Kinetic Mechanism of AKT/PKB Enzyme Family. *J. Biol. Chem. 281*, 13949–13956.
26. Cook, P. F., and Cleland, W. W. (2007) Initial Velocity Studies in the Absence of Added Inhibitors, in Enzyme Kinetics and Mechanism, pp 76−77, Garland Science, New York, NY.
27. Morrison, J. F., and James, E. (1965) The Mechanism of the Reaction Catalysed by Adenosine Triphosphate-Creatine Phosphotransferase. *Biochem. J. 97*, 37–52.
28. Cook, P. F., Neville, M. E., Jr., Vrana, K. E., Hartl, F., T., and Roskoski, R., Jr. (1982) Adenosine Cyclic 3′,5′-Monophosphate Dependent Protein Kinase: Kinetic Mechanism for the Bovine Skeletal Muscle Catalytic Subunit. *Biochemistry 21*, 5794–5799.
29. Midelfort, C. F., and Rose, I. A. (1976) A Stereochemical Method for Detection of ATP Terminal Phosphate Transfer in Enzymatic Reactions. Glutamine Synthetase. *J. Biol. Chem. 251*, 5881–5887.
30. Brouwer, A. C., and Kirsch, J. F. (1982) Investigation of Diffusion-Limited Rated of Chymotrypsin Reactions by Viscosity Variation. *Biochemistry 21*, 1302–1307.
31. Adams, J. A. (2003) Activation Loop Phosphorylation and Catalysis in Protein Kinases: Is There Functional Evidence for the Autoinhibitor Model? *Biochemistry 42*, 601–607.
32. Blacklow, S. C., Raines, R. T., Lim, W. A., Zamore, P. D., and Knowles, J. R. (1988) Triosephosphate Isomerase Catalysis Is Diffusion Controlled. *Biochemistry 27*, 1158–1167.
33. Bossemeyer, D. (1995) Protein Kinases—Structure and Function. *FEBS Lett. 369*, 57–61.
34. Hanks, S. K., Quinn, A. M., and Hunter, T. (1988) The Protein Kinase Family: Conserved Features and Deduced Phylogeny of the Catalytic Domains. *Science 241*, 42–52.
35. Huse, M., and Kuriyan, J. (2002) The Conformational Plasticity of Protein Kinases. *Cell 109*, 275–282.
36. Cleland, W. W. (1975) Partition Analysis and the Concept of Net Rate Constants as Tools in Enzyme Kinetics. *Biochemistry 14*, 3220–3224.
37. Cook, P. F., and Cleland, W. W. (2007) Isotope Effects as a Probe of Mechanism, in Enzyme Kinetics and Mechanism, pp 318−383, Garland Science, New York, NY.
38. Burbaum, J., and Knowles, J. R. (1989) Internal Thermodynamics of Enzymes Determined by Equilibrium Quench: Values of $K_{int}$ for Enolase and Creatine Kinase. *Biochemistry 28*, 9306–9317.
39. Nageswara Rao, B. D., and Cohn, M. E. (1979) $^{31}$P NMR of Enzyme-bound Substrates of Rabbit Muscle Creatine Kinase. Equilibrium Constants, Interconversion Rates, and NMR Parameters of Enzyme-Bound Complexes. *J. Biol. Chem. 256*, 1716–1721.
40. Wilkinson, K. D., and Rose, I. A. (1979) Isotope Trapping Studies of Yeast Hexokinase during Steady-State Catalysis. *J. Biol. Chem. 254*, 12567–12572.
41. Liu, M., Choi, S., Cuny, G. D., Ding, K., Dobson, B. C., Glicksman, M. A., Auerbach., K., and Stein, R. L. (2008) Kinetic Studies of Cdk5/

p25 Kinase: Phosphorylation of Tau and Complex Inhibition of Two Prototype Inhibitors. *Biochemistry 47*, 8367–8377.
42. Wu, H., Zheng, Y., and Wang, Z-x (2003) Evaluation of the Catalytic Mechanism of the p21-Activated Protein Kinase PAK2. *Biochemistry 42*, 1129–1139.
43. Wang, Z-x., and Wu, J-w. (2007) The Complete Pathway for ERK2-Catalyzed Reaction. Evidence for an Iso Random Bi Bi Mechanism. *J. Biol. Chem. 282*, 27678–27684.
44. Kong, C.-T., and Cook, P. F. (1988) Isotope Partitioning in the Adenosine 3′,5′-Monophosphate Dependent Protein Kinase Reaction Indicates a Steady-State Random Kinetic Mechanism. *Biochemistry 27*, 4795–4799.
45. Qamar, R., and Cook, P. F. (1993) pH Dependence of the Kinetic Mechanism of the Adenosine 3′,5′-Monophosphate Dependent Protein Kinase Catalytic Subunit in the Direction of Magnesium Adenosine 5′-Diphosphate Phosphorylation. *Biochemistry 32*, 6802–6806.
46. Tsai, Y-c., and Johnson, K. A. (2006) A New Paradigm for DNA Polymerase Specificity. *Biochemistry 45*, 9675–9687.
47. Litwin, S., and Wimmer, M. J. (1979) Correction of Scrambling Rate Calculation for Loss of Substrate. *J. Biol. Chem. 254*, 1859.